Combustion Process Analysis in a DISI Engine Fuelled with N-Butanol through UV-VIS Emission Spectroscopy

C. Tornatore, A. Irimescu, L. Marchitto, S. S. Merola, and G. Valentino

Abstract—**In this paper, the study on the effects of n-butanol on the combustion process in a DISI engine has been conducted.Experiments were performed on a direct injection SI engine operated on gasoline and butanol, with combined analysis of in-cylinder pressure traces, exhaust emissions and optical data. The optically accessible power unit was fitted with a commercial head and a high pressure wall guided injection system working at 100 bar. The engine speed was set at 2000 rev/min as a representative value for mid-road load automotive use. Different spark timings were tested. All trials were performed at close to stoichiometric air-fuel ratio.UV-visible natural emission spectroscopy was applied to investigate the formation and the evolution of the main compounds characterizing the spark ignition and combustion process. Pollutant measurements (HC, CO and NOx) at undiluted exhaust, for gasoline and butanol, were correlated with pressure related data and optical results.**

Index Terms—**Spark ignition engines, direct injection, butanol, optical investigations.**

I. Introduction

Due to the increasing demand of reducing fossil fuels consumption and the political will to reduce emissions of greenhouse gases, the investigation of alcohols use in spark ignition engines has become interesting in the last years [1]-[3].

While ethanol is the most usual alcohol for automotive applications, butanol is also promising, as its properties are closer to gasoline than those of ethanol. With four carbons, n-butanol contains 25% more energy than ethanol; it is soluble with gasoline in any proportion, whereas the maximum solubility of ethanol in gasoline is around 10% without cosolvents [4]. Butanol has been demonstrated to work in vehicles designed for use with gasoline without modification. It can be produced from the fermentation of the sugars in biomass. Recently, the use of genetically enhanced bacteria increased the fermentation process productivity [5], [6]. It is expected that a sustainable and cost effective process for butanol production will be realized in the foreseeable future.

Recent studies have investigated the use of butanol and its effects on performance [7], [8], emissions [9], [10], injection and spray parameters [11], as well as abnormal combustion [12].

As a general conclusion, the increase in alcohol content in the blend with gasoline, has significant impact on engine performance and efficiency only at high concentrations, if the air-fuel ratio is to be maintained within the same range as for gasoline operation.

Anyway butanol has been studied less extensively than ethanol. Further analyses are necessary to obtain comprehensive information on combustion processes in direct injection (DI) SI engines fuelled with butanol. To this aim, in this paper, integration of experimental methodologies based on conventional (in-cylinder pressure and pollutant exhaust measurements) and unconventional diagnostics (optical techniques) was carried out.

Investigations were performed on a wall guided DISI engine, and pressure related data and exhaust measurements were correlated with UV-visible natural emission spectroscopy data. Commercial gasoline was considered as the reference condition; pure butanol fuelling was compared to the commercial fuel in the mid-engine speed range. Results obtained within these trials can be considered as a valuable database for a better knowledge of the basic combustion mechanisms under realistic engine conditions.

II. Experimental Setup

The engine used for the experiments is an optically accessible single cylinder DISI engine. It is equipped with the head of a commercial SI turbocharged engine with similar geometrical specifications (bore, stroke, compression ratio). The valve overlap on this engine resulted in levels of internal exhaust gas residuals of 5-20%, given that a relatively low intake pressure of ~0.5 bar was set; all trials were performed at 2000 rev/min crank shaft rotational velocity. Further details on the engine are reported in Table I. The head has four valves and a centrally located spark device with surface charge ignition. The injector is side mounted and features 6 holes oriented so that the spray is directed towards the piston crown. Intake air was within 300-310 K and ambient pressure was around 1 atm. Relative air-fuel ratio was measured using a wide band exhaust gas oxygen sensor, with an accuracy of ±1%.

TABLE I: Engine Characteristics

Bore × Stroke	79 × 81.3 mm
Connecting rod length	143 mm
Cylinder	1
Compression ratio	10.6
Fuel system	direct injection 100 bar

For the current work, a conventional elongated hollow Bowditch piston was used. An optical crown, accommodating a 20 mm-thick fused-silica window (57 mm diameter), was screwed onto the piston. The combustion chamber was visible through an UV enhanced 45-degree mirror, mounted within the hollow piston (Fig. 1). Slotted graphite piston rings were used to provide oil-less lubrication

Manuscript received April 20, 2014; revised June 22, 2014.

The authors are with Istituto Motori di Napoli – CNR, Via G.Marconi 4, 80125 Napoli, Italy (e-mail: c.tornatore@im.cnr.it)

with uninterrupted bronze-Teflon rings used for sealing.

Injection pressure was maintained at 100 bar for all conditions; injector opening time was increased when switching from gasoline to butanol. The ratio of 1.21 used for multiplying injection times was determined in order to compensate for the combined effect of lower stoichiometric air-fuel ratio and higher density of butanol (Table II); prior to the experimental trials, a verification was performed using the gravimetric method in order to ensure that changing the fuel did not have an influence on the flow characteristics of the injector. Close to stoichiometric air-fuel mixtures were obtained for all points investigated.

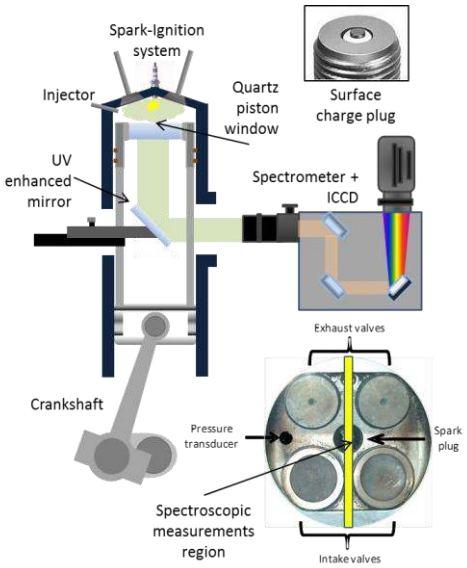

Fig. 1. Experimental setup for optical investigations and bottom field of view of the combustion chamber.

TABLE II: FUEL PROPERTIES

	Gasoline	n-Butanol
Chemical formula	C4 – C12	C4H9OH
Lower heating value (LHV) (MJ/liter)	32.16	26.55
Density (kg/m3)	741	802
Stoichiometric air-fuel ratio (–)	14.7	11.2

Pressure measurements were performed with an accuracy of ±1 % using a piezo-electric transducer, and the correlation with crank angle rotation was done using an encoder with a 0.2 deg resolution; as a result, indicated mean effective pressure (IMEP) was determined with an accuracy of ± 2 %. Unless otherwise stated, all crank angle values are referred to the top dead centre (TDC) at the end of compression. Heat release analysis was performed with a simplified approach, where the ratio of specific heats was chosen as equal to 1.35 [13].

Before the optical investigations, tests with a metallic piston were performed in order to evaluate parameters in a regime as close to steady state operation as possible. A preconditioning unit was used for maintaining the temperature at ~ 340 K during motored operation; during the firing cycles, a variation of ~ 5 K was recorded for both average values.

Exhaust gas concentrations were determined with a gas analyser using the non-dispersive infrared measurement principle for carbon monoxide (CO) and unburned hydrocarbons (HC), while for nitrogen oxides (NO_x) emissions, the electrochemical method was employed. Accuracy was within ±3 % and the resolution of the readings for the first component was 0.01% and 1 ppm for the other two species.

During the UV-visible spectroscopy experiments, the radiative emission from the combustion chamber was focused by a 78 mm focal length, f/3.8 UV Nikon objective onto the 250 µm micrometer controlled entrance slit of a spectrometer with 150 mm focal length and 300 groove/mm grating (central wavelength 350 nm). From the grating, the radiations were detected by an intensified CCD camera (array size of 1024 x 1024 pixels with a pixel size of 13×13 µm, 16-bit pixel digitization and 1MHz sustained repetition rate). A sequential gating mode was used to study the temporal evolution of the flame propagation: it allowed to collect one frame per cycle with fixedgate width but variable delay with respect to the trigger. Spectra were recorded for 100 consecutive cycles, at a step of 1 deg crank angle (83 µs), with an exposure time of 83 µs. Spectroscopic investigations were carried out in the central region of the combustion chamber. The emission spectra were corrected for the wavelength dependent sensitivity of the optical devices. The wavelength calibration was performed using a mercury lamp. Spectroscopic data post-processing allowed to evaluate the time evolutions of chemical species featuring the combustion process in all the operative conditions. It should be noted that all the detected species through emission spectroscopy are in excited electronic states; for this reason the notation "*" that identifies the excited species will be omitted. In this work, for each individual-cycle spectrum, OH, CH and CO_2 emission were evaluated at 309, 390 and 431 nm relative to the local background, which was estimated by linear interpolation between the nearest intensity minima on either side of the band containing the feature of interest.

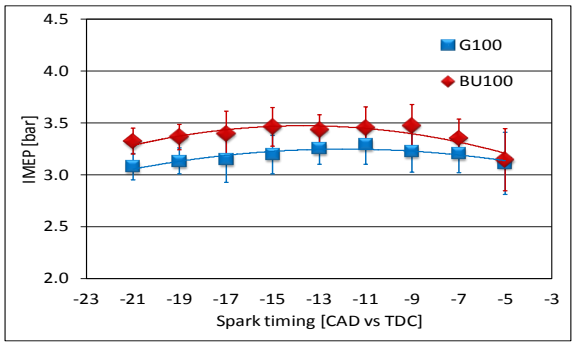

Fig. 2. Indicated mean effective pressure (IMEP) at different spark timing settings. Standard deviations are reported as error bars.

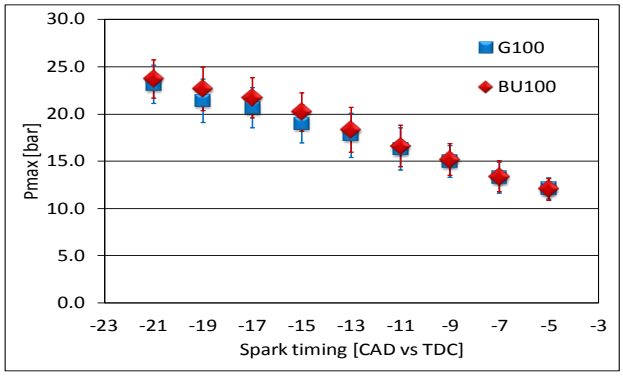

Fig. 3. Peak pressure at different spark timing settings. Standard deviations are reported as error bars.

III. Results and Discussions

A. Thermodynamic Analysis

In order to evaluate the effect of the spark advance on the engine performance, the values of the mean effective pressure (IMEP) and of the peak pressure (Pmax) at different spark timing settings were measured. The results obtained by averaging the values related to 200 consecutive engine cycles are reported in Fig. 2 and Fig. 3. The analysis allowed determining 13 CAD BTDC as the spark timing correspondingto the maximum brake torque (MBT) for each fuel. IMEP was found to be quite flat around the MBT point. Cyclic variability was evaluated through the standard deviation and it was reported in the plots as error bars. IMEP differences between the two fuels were within ± 8 %, with higher values for the butanol throughout the studied spark timing range. The increase in the Pmax values with the increase of the spark advance was higher for butanol. This determines very close peaks of pressure at delayed spark timing and appreciable difference only beyond 13 CAD BTDC.

Regarding the exhaust emissions, Figs. 4-6 reported the concentration at undiluted exhaust of CO, HC and NO_x measured at different spark timings. Minor differences were recorded for carbon monoxide emissions (Fig. 4) when switching from gasoline to butanol, even if butanol gives slightly higher CO emissions. Decreasing in CO post-flame oxidation is responsible for this [9].

Unburned hydrocarbons concentrations in the exhaust gas stream were reported in Fig. 5.

When retarding the spark timing, HC emissions decrease for gasoline; for butanol the reduction is evident in the range -19 -13 CAD, then there is a quite constant value between -13 and -5 CAD. The decrease in HC at delayed spark timing happens because, when spark timing is postponed, both the average cylinder temperature of post-flame and exhaust gas temperatureincrease, resulting in the promotion of in-cylinder unburned hydrocarbon oxidation. In addition, as spark timing is delayed, the peak cylinder pressure decreases and the mass fraction of HC trapped in the crevice volumes is reduced.

The slight increase in HC emissions when using butanol in delayed spark timing conditions is due to the characteristics of butanol that shows higher boiling temperature and latent heat of vaporization, thus it is the slowest to vaporize. This induces a decreased combustion efficiency resulting in higher HC emissions.

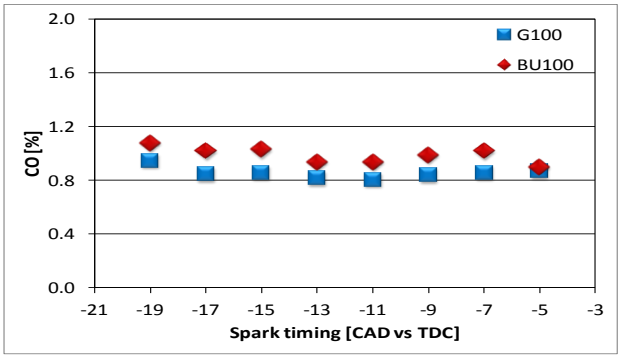

Fig. 4. CO emission for different spark timing settings.

Spark timing significantly affects NO_x emission levels. Advancing the spark timing makes early combustion and increases the cylinder peak pressure. Combustion temperature and local oxygen concentrations are the major factors affecting NO_x formation. An increase in-cylinder peak pressures corresponds to an increase in-cylinder peak temperature, leading to an increase in NO_x emissions [9].

Considerably lower NO_x concentrations in the exhaust gas stream when using butanol were detected. Lower NO_x emissions when using the alcohol are in line with the findings of most studies about butanol combustion in SI engines [14]-[16].The reduction in *NOx* emissions is due to the low adiabatic temperature when engine operates on butanol.

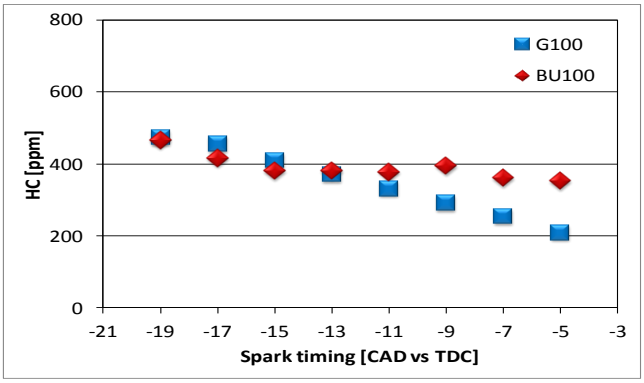

Fig. 5. HC emission for different spark timing settings.

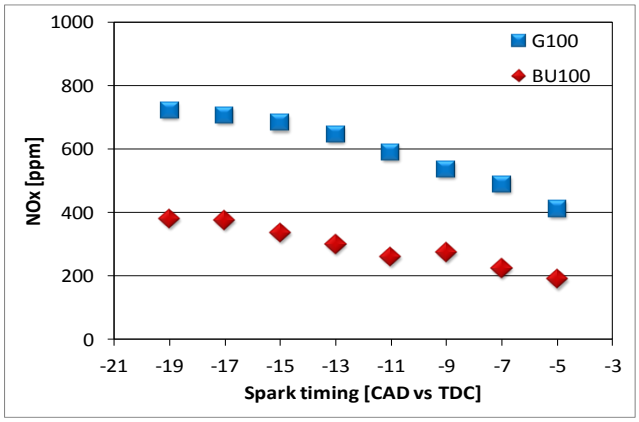

Fig. 6. NOx emission for different spark timing settings.

B. Spectroscopic Investigations

In this work, UV-visible natural emission spectroscopy was applied starting from the spark ignition for both fuels fixing ignition advance at MBT spark timing (13 CAD BTDC). Fig. 7 shows spectra acquired in the spark plug region for the two fuels within the first CAD after the spark timing. The spark discharge forms a plasma featured by CN, NH and OH radicals [17]. Moreover weak emission band systems, due to high degree ionization and dissociation of nitrogen, are detectable [18]. The electronically excited CN is generally identified by the $B^2\Sigma^+ \rightarrow X^2\Sigma^+$ bands due to the diagonal transitions (Δv=0). These are well resolved in the 380–390 nm spectral range with highest peak at 388 nm [19]. Weaker band systems due to the Δv=+/-1 transitions were observed around 357 and 420 nm. The emission of systems of N_2 and N_2^+ emission can be strongly unstable [20]. N_2 is featured by a weak band around 337 nm and 313 nm due to $C^3\Pi \rightarrow B^3\Pi$ (0, 0) and (0, 1) transitions [21]. N_2^+ emission is characterized by red band systems due to $B^2\Sigma^+ \rightarrow X^2\Sigma^+$

transitions in the 330-435 nm range [22]. The most intense peak is at 391 nm (0, 0) but the other systems are resolvable through their local maxima at 357 nm (1,0) and 428 nm (0,1). The $A^3\Pi \rightarrow X^3\Sigma^-$ transition of NH induces diffuse bands between 325 and 340 nm with a well-defined peak at 338 nm [23]. Due to the overlapping of the emission bands, it is hard to distinguish the plasma emission contribution due to the different chemical species.

Regarding the presence of OH radicals in the plasma emission at the spark timing, it is correlated to the formation of filamentary discharge [24]. OH radicals, as O and H atoms, are key species for the initiation of combustion since they are the main species responsible for breaking C–H bonds in hydrocarbon fuels [25]. OH emission is characterized by a violet band system centred at 309 nm due to the$A^2\Pi \rightarrow X^2\Pi$ transition [26], [27]. The dominant feature is the (0,0) vibrational band (peak at 306 nm). A second band system (1,0) with the peak at 282 nm is too weak to be well resolved.

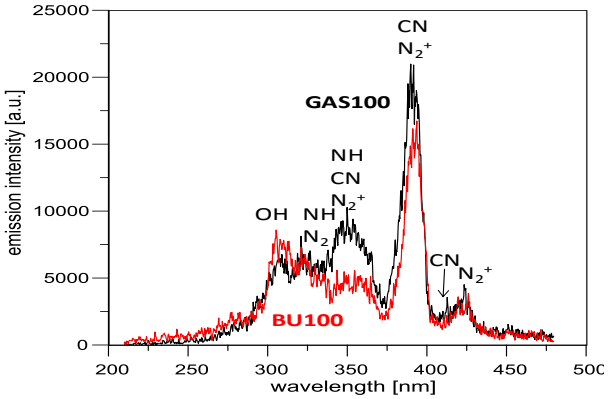

Fig. 7. Emission spectra detected in the combustion chamber central region at the spark timing.

After the spark timing, the first well resolved spectral signals due to the flame kernel emission were observed almost at 5 CAD after the spark timing when the plasma emission intensity was strongly decreased. As shown in Fig. 8, for both fuels, kernel spectra were featured by OH band systems at 309 nm [28]. Moreover, CH emission band can be resolved.CH emission bands are well known and have been observed by several researchers in hydrocarbon flames, discharge tubes containing carbon and hydrogen, as well as carbon arcs in hydrogen. The most intense is the (0,0) $A^2\Delta \rightarrow X^3\Pi$ band with the peak at 431 nm [29]. A weaker band can be observed from 387 to 491 nm with the local maximum at 389 nm due to the (0,0) $B^2\Sigma^- \rightarrow X^2\ \Pi$ transition [30].

The total emission intensity is higher for gasoline. This confirms a faster kernel inception due to higher local fuel-air ratio. Moreover, while the OH bands at 309 nm were comparable, CH bands resulted more intense for gasoline. These results are correlated to higher local fuel/air ratio for gasoline compared to butanol [31]. Since the overall air-fuel ratio measured by lambda sensor was the same, this result demonstrated a different spatial distribution of the charge.

In the spectra detected in early combustion stages (Fig. 8), OH and CH bands were superimposed on two broad overlapped band systems. The first was due to the Emeleus cool flame band system of HCOH that lies between 340 and 520 nm with its highest peak around 390 nm. The second broad band identified the Vaidya hydrocarbon system of HCO that spreads over 250-410 nm. Formaldehyde and formyl radicals are directly correlated to CH production through the decomposition of the HCO radical and the hydrogen peroxide formation [31].

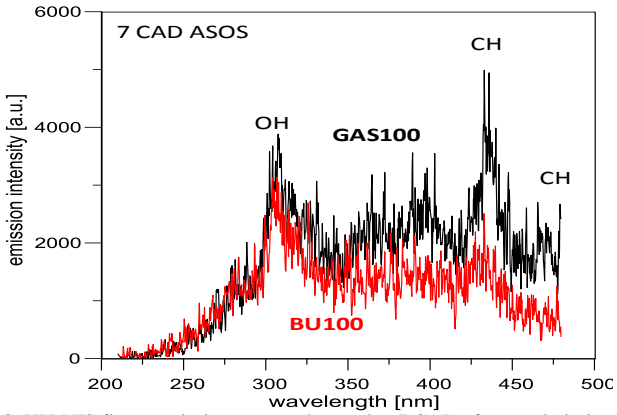

Fig. 8. UV-VIS flame emission spectra detected at 7 CAD after spark timing (CAD ASOS).

As shown in Fig. 9, at 15 CAD ASOS the two fuels showed similar spectral features and intensities. With higher OH and lower CH emissions for butanol compared to gasoline. This occurrence is in agreement with the thermodynamic results reported in Table III which correlate with flame speed that for butanol is higher than that of gasoline. It should be noted that the end of combustion was considered as the point where flame development is completed (i.e. 400 CAD, when the mixture within the combustion chamber is consumed), without the final part of the process, which features mainly oxidation of unburned mixture flowing from the crevices into the cylinder, as well as fuel deposits. Moreover, around this time (i.e. at 15 CAD ASOS), spectral features due to excited CO_2 were observed. As known, the flame emission after initiation is characterized by the radiative reaction of atomic oxygen and carbon monoxide. It shows a strong blue continuum between 250 and 800 nm with a maximum intensity around 400 nm in [32]. This emission is due to the chemiluminescence accompanying the recombination of CO and O:

$$CO\ (X^1\Sigma^+) + O\ (A^3\Pi) \rightarrow CO_2\ (X^1\Sigma^+_g) + h\nu$$

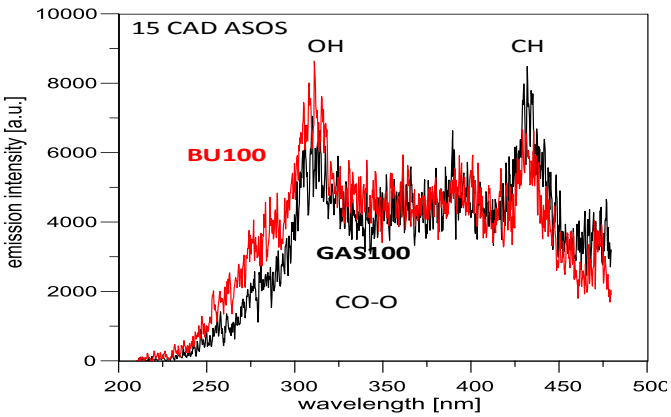

Fig. 9. UV-VIS flame emission spectra detected at 15 CAD after spark timing (CAD ASOS).

Following the combustion process, the spectra evolved in intensity, that increased, and features. For both fuels, CH

disappeared showing strong OH emission superimposed to the CO_2 wide band. Around 25 CAD after spark (Fig. 10), gasoline presented higher CO_2 and comparable OH emissions to butanol. This agrees with the OH contribution to the oxidation of CO in CO_2 [33].

As shown in Fig. 11, at 35 CAD ASOS, a weak continuous signal that increased with the wavelength similar to blackbody curve was observed for gasoline. This was due to soot precursors emission formed during the burning of the fuel deposits in the combustion chamber. Moreover, OH resulted slightly higher for butanol, that was also featured by the (1,0)$A^2\Pi \rightarrow X^2\Pi$ transition at 282 nm.

TABLE III: THERMODYNAMIC PARAMETERS MEASURED CONSIDERING 13 CAD BTDC AS SPARK TIMING

fuel	CAD Pmax [ATDC]	CAD 0.1 MFB [ATDC]	CAD 0.5 MFB [ATDC]	CAD 0.9 MFB [ATDC]
BU100	23.4	5.6	20.5	46.5
G100	24.9	4.7	21.1	47.7

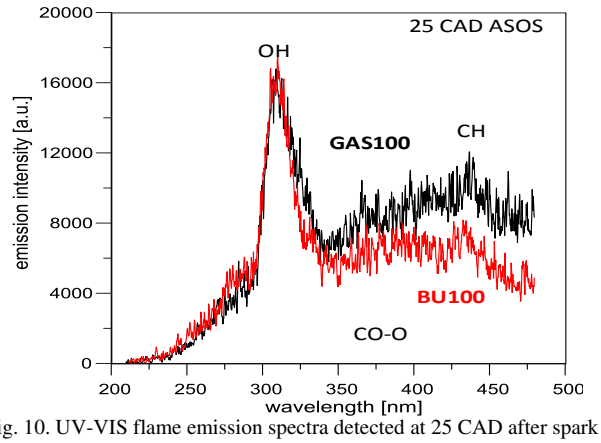

Fig. 10. UV-VIS flame emission spectra detected at 25 CAD after spark timing (CAD ASOS).

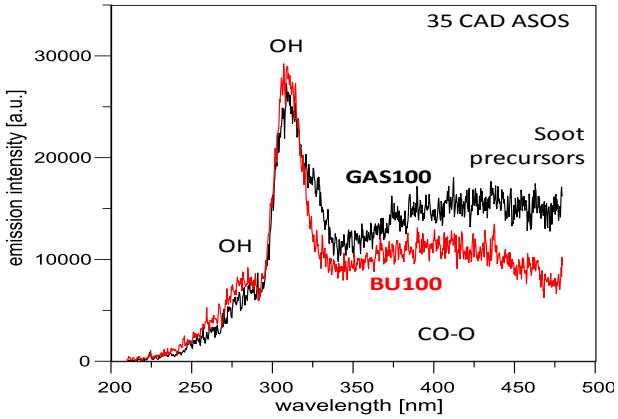

Fig. 11. UV-VIS flame emission spectra detected at 35 CAD after spark timing (CAD ASOS).

At 45 CAD ASOS, the soot signal is very intense for gasoline, as shown in Fig. 12. Moreover, in gasoline spectra soot emission is still significant at 55 CAD ASOS (Fig. 13). These results demonstrate that the fuel deposits flames persisted well after the normal combustion event. In the late combustion phase, soot was not detectable for butanol, indicating the potentiality of this fuel in reaching smokeless targets. At 55 CAD ASOS, butanol combustion was completed in agreement with the thermodynamic results reported in Table III.

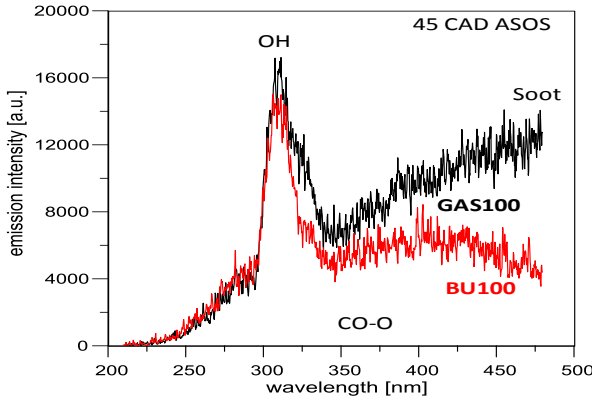

Fig. 12. UV-VIS flame emission spectra detected at 45 CAD after spark timing (CAD ASOS).

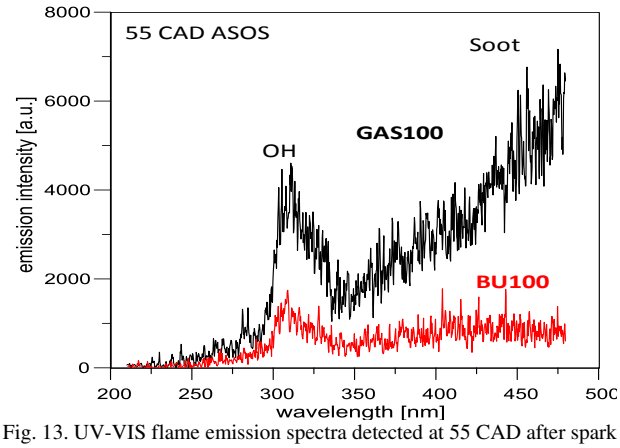

Fig. 13. UV-VIS flame emission spectra detected at 55 CAD after spark timing (CAD ASOS).

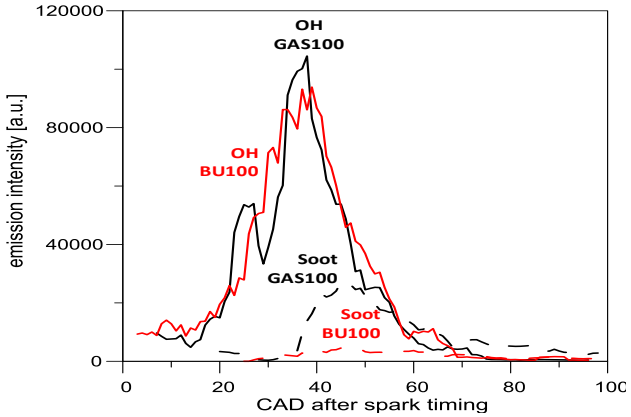

Fig. 14. OH radicals and soot evolution evaluated from flame emission spectroscopy.

Experimental investigations demonstrated that excited OH radical was a marker of spark ignited flame propagation for gasoline and butanol [34], [35]. The maximum intensity and total amount of OH emission, and as consequence the flame speed towards the combustion chamber walls, increased with the spark advancing and decreased with the air-fuel ratio increase.

In this work, time evolution of OH radicals and soot evaluated from spectroscopic data for both fuels are plotted in Fig. 14. Spectroscopic investigations demonstrated very low level of soot emission intensity in the combustion chamber, confirming the low opacity measured at the exhaust due to

butanol (opacity for BU100=1.2%, opacity for G100=3.4%). On the other side, OH emissions resulted comparable for the two fuels.

IV. Conclusions

UV-visible natural emission spectroscopy was applied in a SI engine optically accessible to investigate the potentiality of n-butanol as gasoline replacement at low speed and load in stoichiometric mixture conditions.

The general conclusion is that the reference fuel can be replaced with the four carbon atoms alcohol in DISI engines without any penalty on performance. Even more, reductions of several exhaust emissions were obtained when using the alternative fuel.

One of the main advantages of replacing the butanol with the gasoline is the strong reduction in smoke opacity. Regarding HC emissions, using the alternative fuel resulted in an increase but only for delayed spark timing. On the contrary, nitrogen oxides concentration in the exhaust gas stream was lower for butanol for each spark timings.

Acronyms and Abbreviations

ASOS	after start of spark
a.u.	arbitrary unit
BU100	butanol
CAD	crank angle degree
ICCD	intensified charge coupled device
COV	coefficient of variation
DI	direct injection
GAS100	gasoline
IMEP	indicated mean effective pressure, (bar)
MBT	maximum brake torque
LHV	lower heating value
MFB	mass fraction burned
P	pressure, (bar)
Pmax	peak pressure, (bar)
SI	spark ignition
TDC	top dead centre, with A for after and B for before
VIS	visible
UV	ultraviolet

Acknowledgment

The authors are grateful to Mr. Alfredo Mazzei for the optical engine assessment and for the technical support to the experiments.

References

[1] Z. Zhang, T. Wang, M. Jia, Q. Weia, X. Meng, and G. Shua, "Combustion and particle number emissions of a direct injection spark ignition engine operating on ethanol/gasoline and n-butanol/gasoline blends with exhaust gas recirculation," *Fuel*, April 2014.

[2] B. G. Harvey and H. A. Meylemans, "The role of butanol in the development of sustainable fuel technologies," *J Chem Technol Biotechnol*, vol. 86, pp. 2-9, 2011.

[3] K. R. Szulczyk, "Which is a better transportation fuel – Butanol or ethanol?" *Int J Energy Environ*, vol. 1, pp. 501-512, 2010.

[4] B. Yang, M. Yao, W. K. Cheng, Z. Zheng, and L. Yue, "Regulated and unregulated emissions from a compression ignition engine under low temperature combustion fuelled with gasoline and n-butanol/gasoline blends," *Fuel*, vol. 120, no. 15, pp. 163-170, March 2014.

[5] S. Baba, Y. Tashiro, H. Shinto, and K. Sonomoto, "Development of high-speed and highly efficient butanol production systems from butyric acid with high density of living cells of clostridium saccharin perbuty lacetonicum," *J Biotechnol*, vol. 157, pp. 605-612, 2012.

[6] Y. Jang, A. Malaviya, C. Cho, J. Lee, and S. Y. Lee, "Butanol production from renewable biomass by clostridia," *Bioresource Technol*, vol. 123, pp. 653-663, 2012.

[7] B. Deng, J. Yang, D. Zhang *et al*., "The challenges and strategies of butanol application in conventional engines: The sensitivity study of ignition and valve timing," *Applied Energy*, vol. 108, pp. 248-260, 2013.

[8] T. Venugopal and A. Ramesh, "Experimental studies on the effect of injection timing in a SI engine using dual injection of n-butanol and gasoline in the intake port," *Fuel*, vol. 115, pp. 295-305, 2014.

[9] X. Gu, Z. Huang, J. Cai, J. Gong, X. Wu, and C. Lee, "Emission characteristics of a spark-ignition engine fuelled with gasoline-n-butanol blends in combination with EGR," *Fuel*, vol. 93, pp. 611-617, 2012.

[10] G. Broustail, F. Halter, P. Seers, G. Moréac, and C. Mounaim-Rousselle, "Comparison of regulated and non-regulated pollutants with iso-octane/butanol and iso-octane/ethanol blends in a port-fuel injection spark-ignition engine," *Fuel*, no. 94, pp. 251-261, 2012.

[11] J. S. Pereira, P. G. Aleiferis, and D. Richardson, "Imaging and heat flux measurements of wall impinging sprays of hydrocarbons and alcohols in a direct-injection spark-ignition engine," *Fuel*, vol. 91, pp. 264-297, 2012.

[12] S. S. Merola, G. Valentino, C. Tornatore, and L. Marchitto, "In-cylinder spectroscopic measurements of knocking combustion in a SI engine fuelled with butanol–gasoline blend," *Energy*, vol. 62, pp. 150-161, 2013.

[13] J. B. Heywood, *Internal Combustion Engine Fundamentals*, New York, USA: McGraw Hill, 1988.

[14] J. Dernotte, C. M. Rousselle, F. Halter, and P. Seers, "Evaluation of butanol-gasoline blends in a port fuel-injection spark-ignition engine," *Oil Gas Sci. Technol.*, vol. 65, pp. 345-351, 2010.

[15] S. Szwaja and J. D. Naber, "Combustion of n-butanol in a spark-ignition IC engine," *Fuel*, vol. 89, pp. 1573-1582, 2010.

[16] T. Venugopal and A. Ramesh, "Effective utilisation of butanol along with gasoline in a spark ignition engine through a dual injection system," *Applied Thermal Engineering*, vol. 59, pp. 550-558, 2013.

[17] Q. S. Yu and H. K. Yasuda, "An optical emission study on expanding low-temperature cascade arc plasmas," *Plasma Chemistry and Plasma Processing*, vol. 18, pp. 461-485, 1998.

[18] R. M. Merer and J. S. Wallace, "Spark spectroscopy for spark ignition engine diagnostics," SAE Paper, 1995.

[19] D. Cerny, R. Bacis, G. Guelachvili, and F. Roux, "Extensive analysis of the red system of the CN molecule with a high resolution spectrometer," *Journal of Molecular Spectroscopy*, vol. 73, no. 1, pp. 154-167, October 1978.

[20] R. F. Wuerker, L. Schmitz, T. Fukuchi, and P. Strauss, "Lifetime measurements of the excited states of N2 and N2+ by laser-induced fluorescence," *Chemical Physics Letters*, vol. 150, no. 6, pp. 443-446, September 1988.

[21] H. Nassar, S. Pellerin, K. Musiol, O. Martinie, N. Pellerin, and J. -M. Cormier, "N2+/N2 ratio and temperature measurements based on the first negative N2+ and second positive N2 overlapped molecular emission spectra," *J. Phys. D: Appl. Phys*., vol. 37, pp. 1904-1916, 2004.

[22] L. Klynning and P. Pages, "The band spectrum of N2+," *Phys. Scripta*, vol. 25, pp. 543, 1982.

[23] K. Fukui, I. Fujita, and K. Kuwata, "Formation of the NH (A3Π-clΠ) radicals by electron impact near threshold," *The Journal of Physical Chemistry*, vol. 81, pp. 1252-1257, 1977.

[24] G. Pilla, D. Galley, D. A. Lacoste, F. Lacas, D. Veynante, and C. O. Laux, "Stabilization of a turbulent premixed flame using a nanosecond repetitively pulsed plasma," *IEEE Transactions on Plasma Science*, vol. 34, no. 6, pp. 2471-2477, 2006.

[25] J. L. Jauberteau, I. Jauberteau, M. J. Cinelli, and J. Aubreton, "Reactivity of methane in a nitrogen afterglow," *New J. Phys.*, vol. 4, pp. 1-13, 2002.

[26] G. H. Dieke and H. M. Crosswhite, "The ultraviolet bands of OH," *J. Quant. Spectrosc. Radiat.Transfer*, vol. 2, pp. 97-199, 1962.

[27] J. Luque and R. Crosley, "Transition probabilities in the A2Π →X2Π electronic system of OH," *J. Chem. Phys*., vol. 109, pp. 439-449, 1998.

[28] C. Th. J. Alkemade and R. Herrmann, *Fundamentals of Analytical Flame Spectroscopy*, Bristol, UK: Hilger, 1979.

[29] J. Luque and D. R. Crosley, "Electronic transition moment and rotational transition probabilities in the CH A-X system," *J. Chem. Phys.*, vol. 104, pp. 2146-2155, 1996.

[30] J. Luque and D. R. Crosley, "Electronic transition moment and rotational transition probabilities in the CH A-X system," *J. Chem. Phys.*, vol. 104, pp. 3907-3913, 1996.

[31] A. G. Gaydon and H. G. Wolfhard, "Mechanism of formation of CH, C2, OH and HCO radicals in flames," in *Proc. Symposium (International) on Combustion*, vol. 4, no. 1, pp. 211-218, 1953.
[32] G. F. Kirkbright and T. S. West, "The Application of Separated Flames in Analytical Flame Spectroscopy," *Appl. Opt.*, vol. 7, pp. 1305-1311, 1968.
[33] C. T. Bowman, "Kinetics of pollutant formation and destruction in combustion," *Progress in Energy and Combustion Science*, vol. 1, pp. 33-45, 1975.
[34] C. Tornatore, S. Merola, G. Valentino, and L. Marchitto, "In-cylinder spectroscopic measurements of combustion process in a SI engine fuelled with butanol-gasoline blend," SAE Technical Paper, 2013.
[35] S. S. Merola, L. Marchitto, C. Tornatore, G. Valentino, and A. Irimescu "UV-visible optical characterization of the early combustion stage in a DISI engine fuelled with butanol-gasoline blend," *SAE International Journal of Engines*, vol. 6, no. 4, 2013.

Cinzia Tornatore was born in 1980. She received her magister degree in chemical engineering from the University of Naples in Italy, 2004. She received her PhD in chemical engineering in 2007. Her education activities were focused on the optical diagnostics of nanoparticles at internal combustion engines exhaust. From 2007 to 2011 she worked as an associate researcher at Istituto Motori of "Italian National Research Council". Since 2011 she is a tenured researcher and she is involved in research projects on the optical characterization of combustion process in internal combustion engines.

Adrian Irimescu received his degree in mechanical engineering in 2004, at the end of five year courses at the Politehnica University of Timisoara, Romania; he pursued a master's degree on the energy and environmental aspects of combustion equipment. Following a three year period, he received his PhD in mechanical engineering in 2009, after which, between 2010 and 2013 he developed research into the use of alternative fuels in internal combustion engines within the framework of a postdoctoral grantat the same institution. He is currently studying the application of butanol and other unconventional energy sources in spark ignition engines at the Istituto Motori Napoli, Italy.

Luca Marchitto got the mechanical engineering MD at the University of Naples in Italy in 2006 working on fuel injection apparatuses for HD diesel engines. Since 2006. he is associate researcher at Istituto Motori of "Italian National Research Council". His activity is mainly focused on fluid-dynamic characterization of sprays and high injection pressure combustion by non-intrusive techniques using both mineral and biodegradable (first and second generation) fuels. He use currently optical (Imaging, PDPA, PIV, UV-VIS chemiluminescence techniques) and non conventional techniques (X-Rays) as well as forecast simulating codes to study mechanisms influencing the air/fuel mixture formation in internal combustion engines.

Simona Silvia Merola received her magister degree in physics from the University of Naples in Italy in 1995 and she received her PhD in chemical engineering in 2000. Since 2001 she has been a researcher in istituto motori of the Italian National Research Council, specializing in the application of optical diagnostics to the combustion process investigation. Her research work is focused on the experimental analysis of the thermo fluid-dynamic phenomena that occur in-cylinder and at the exhaust of the internal combustion engines. Since 1996, she has been involved with and has the direct responsibility for experimental activities in several national and international research projects.

Gerardo Valentino was born in 1957. He received his master degree with honour in mechanical engineering from the University of Naples "Federico II" in 1980. He joined Istituto Motori (IM) of National Research Council (CNR) as researcher in 1984. In 2006 he was promoted to the rank of research manager and currently is overseeing one of the divisions of Istituto Motori focused on the mixture formation process and combustion within direct injection engines. Dr. Valentino is the author of a large number of papers in qualified scientific conferences and magazines with more than 20 years of expertise in optical diagnostics for fluid-dynamic and spray combustion research in internal combustion engines.